ACS APPLIED MATERIALS & INTERFACES

Research Article

www.acsami.org

Formation of Interfacial Layer and Long-Term Cyclability of Li–O_2 Batteries

Eduard N. Nasybulin,[†] Wu Xu,*[,†] B. Layla Mehdi,[‡] Edwin Thomsen,[†] Mark H. Engelhard,[§] Robert C. Massé,[†,∥] Priyanka Bhattacharya,[†] Meng Gu,[§] Wendy Bennett,[†] Zimin Nie,[†] Chongmin Wang,[§] Nigel D. Browning,[‡] and Ji-Guang Zhang*[,†]

[†]Energy and Environment Directorate, [‡]Fundamental and Computational Sciences Directorate, [§]William R. Wiley Environmental and Molecular Sciences Laboratory, Pacific Northwest National Laboratory, Richland, Washington 99354, United States

[∥]Department of Chemical and Biological Engineering, University of Wisconsin–Madison, Madison, Wisconsin 53706, United States

Supporting Information

ABSTRACT: The long-term operation of Li–O_2 batteries under full discharge/charge conditions is investigated in a glyme-based electrolyte. The formation of stable interfacial layer on the electrode surface during the initial cycling stabilizes reaction products at subsequent cycling stages as demonstrated by quantitative analyses of the discharge products and the gases released during charging. There is a quick switch from the predominant formation of Li_2O_2 to the predominant formation of side products during the first few cycles. However, after the formation of the stable interfacial layer, the yield of Li_2O_2 in the reaction products is stabilized at about 33–40%. Extended cycling under full discharge/charge conditions is achievable upon selection of appropriate electrode materials (carbon source and catalyst) and cycling protocol. Further investigation on the interfacial layer, which in situ forms on air electrode, may increase the long-term yield of Li_2O_2 during the cycling and enable highly reversible Li–O_2 batteries required for practical applications.

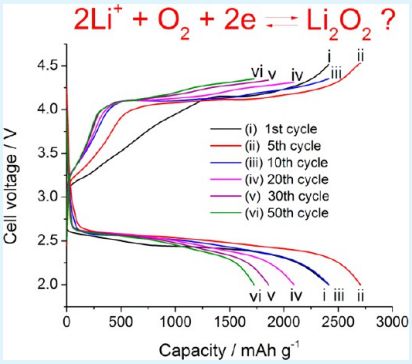

KEYWORDS: *Li–O_2 battery, rechargeability, carbon nanotubes, Li_2O_2, cyclability*

1. INTRODUCTION

High-density energy storage systems have been intensively investigated worldwide in recent years in response to the increased need for long-range electric vehicle and large scale renewable energy applications. Conventional Li-ion batteries still cannot fully satisfy these ever-increasing needs because of their limited energy density, high cost, and safety concerns. As an alternative, the rechargeable Li–O_2 battery has been widely recognized as a promising candidate for the next generation energy storage systems.[1] The theoretical energy density of a Li–O_2 battery is ~3500 Wh kg^{-1} (including the mass of Li_2O_2 as a discharge product), which is significantly higher than many other battery systems.[2] However, a rechargeable Li–O_2 battery suitable for practical applications has not been realized since the concept was first reported by Abraham and Jiang in 1996.[3] The most critical barrier in the development of practical Li–O_2 batteries is decomposition/side reactions on the electrode/electrolyte interface. Reduced oxygen (O_2) species generated during the operation of the Li–O_2 battery[4] are highly reactive with nearly every component inside the battery, and they lead to insoluble lithium alkyl carbonates and Li_2CO_3.[5−7] Although glyme-based solvents are more stable than carbonate-based solvents, they also exhibit clear degradation during the discharge/charge processes in an O_2-rich environment.[8−10] Other less commonly used solvents also exhibit various degrees of degradation when used in Li–O_2 batteries.[10−13] In addition to solvents, most lithium salts also are prone to decomposition in the Li–O_2 battery environment as revealed by several recent studies.[14−16] Moreover, carbon-based air electrodes have been found to be reactive both chemically and electrochemically during Li–O_2 battery operation.[17−20] Bruce and co-workers reported that a carbon electrode undergoes minor decomposition during discharge while exhibiting severe decomposition during the charging process above 3.5 V with the formation of Li_2CO_3 which partially decomposed to release CO_2 during subsequent charging process.[19] In addition to carbon decomposition, other components of the cathode, such as the catalyst or binder, also may contribute to the degradation of the electrode/electrolyte interface.[21−23]

Although the decomposition pathways for common electrolytes and carbon electrodes have been suggested and decomposition products were well characterized, several groups reported stable discharge/charge of Li–O_2 batteries for 50–100 cycles.[24−26] Such cycling is typically realized under certain conditions, such as capacity-limited cycling (which often uses less than 10% of the full discharge capacities). Except for a few cases (e.g., when nanoporous gold or TiC were used as air electrodes),[27,28] most Li–O_2 batteries reported today can retain

Received: June 3, 2014
Accepted: July 28, 2014
Published: July 28, 2014

less than 50% of the original capacity after ~10 cycles when they are fully discharged. Another common issue in literature reports on the rechargeable Li−O_2 batteries is a lack of comprehensive characterization. Some of methods suitable for bulk analysis are difficult to be used to analyze the small amounts of products generated during discharge of the cycled electrodes, which typically have low loadings. In some cases, the highly reversible Li−O_2 batteries have been claimed based on capacity-limited protocols and the presence of Li_2O_2 identified during the first few cycles, although there is no further experimental support that the similar amount of Li_2O_2 is also generated during the long-term cycling. On the other hand, the reversibility of Li−O_2 batteries is often reported based on qualitative information rather than quantitative analysis of Li_2O_2. To address this problem, McCloskey et al.[20] recently reported an accurate quantitative analyses of the reaction products produced during the first discharge/charge cycle in a 1,2-dimethoxyethane (DME)-based electrolyte. In another study, Ottakam et al.[19] showed an increasing amount of Li_2CO_3 in discharge products over the first five cycles of battery operation. However, detailed analyses of the reaction products of Li−O_2 batteries during long-term, full capacity cycling as well as the conditions needed to achieve this long-term cycling have not been described in the literature.

In this work, we investigated the conditions that lead to long cycle life of Li−O_2 batteries. Contributions from both desired Li−O_2 reactions and undesired side reactions to the total capacities are analyzed with quantitative support during extended cycling. The interplay between the yields of Li_2O_2 and the side products produced during cycling is discussed in relation to the changes on the electrode/electrolyte interface. The origin and role of the side products and their decomposition conditions are also analyzed.

2. EXPERIMENTAL SECTION

2.1. Chemicals. Tetraethylene glycol dimethyl ether (tetraglyme), 1,2-dimethoxyethane (DME), lithium trifluoromethanesulfonate (LiTf) were ordered in battery grade from BASF. Lithium chips were obtained from MTI Corporation. These chemicals were stored in an Ar-filled glovebox (MBraun). Carbon nanotubes (CNTs, SWCNT/DWCNT, >90%) were purchased from CheapTubes. Ruthenium(III) chloride, sodium dodecyl sulfate (SDS), and glycerol were ordered form Sigma-Aldrich and used as received. Lithiated Nafion (Lithion) was purchased from IonPower.

2.2. Preparation of CNTs/Ru Nanocomposites. Dispersed CNTs were decorated with Ru nanoparticles by thermal reduction of $RuCl_3$ in the glycerol/H_2O mixture. CNTs are commonly dispersed in aqueous solutions through a carboxylation step.[29] However, application of carboxylated CNTs was found to significantly decrease the discharge capacity of the CNTs/Ru electrodes, apparently because carboxylation required a strong oxidizing acidic medium and resulted in chopping of CNTs,[29] thereby decreasing the active surface area of the final CNTs/Ru composite. Instead, solubilization of CNTs was effectively done using SDS.[30]

The method for the preparation of CNTs/Ru composite was adopted from the literature.[30,31] CNTs (200 mg) were dispersed in the solution of 50 mg SDS in 35 mL of deionized water under mild sonication (15 min). Next, 105 mL of glycerol/water mixture (3:1 volume ratio) was added and the suspension was subjected to additional mild sonication (30 min). A solution of $RuCl_3$ (400 mg) in 80 mL of a glycerol/water mixture was prepared in another flask and added dropwise to the stirred suspension of CNTs. After that, the mixture was subjected to reflux for 5 h. The CNTs/Ru composite was collected by filtration on a Buchner funnel followed by washing with deionized water and drying in oven at 100 °C.

2.3. Electrode Preparation, Battery Assembly, and Testing. CNTs or CNTs/Ru powder (20.0 mg) was dispersed in 1.00 g of a 10 wt % solution of Lithion in methanol with the help of a homogenizer. The prepared slurry was evenly deposited on a 5 cm × 10 cm sheet of Teflon treated carbon paper (Toray, TGP-H-030) serving as the gas diffusion layer and current collector so that the total loading of CNTs or CNTs/Ru was about 0.4 mg cm^{-2}. Electrode disks with loading of about 0.6 mg (i.e., disk rea of 1.6 cm^2) were die cut and dried in a vacuum oven at 80 °C for 24 h.

Batteries were assembled in perforated coin cell stainless steel cases (CR2032) inside the Ar-filled MBraun glovebox. Carbon paper faced the perforated side of the cell and the active layer faced the Celgard 2500 separator. One piece of glass fiber separator (GF/B, Whatman) soaked with 300 μL of electrolyte (1.0 M LiTf in TEGDME) was placed on top of the Celgard membrane so that the membrane prevented glass fibers from sticking to the active layer. Li foil was used as an anode.

The assembled batteries were tested in airtight Teflon containers filled with ultrahigh purity O_2 (1 atm) at a constant current density of 0.10 mA cm^{-2} (0.16 mA per electrode disk). In our tests, the low limit of discharge voltage was set at 2 V where the Li−O_2 battery normally reaches its fully discharged state. The charge capacity was controlled to be equal to the discharge capacity so the reversibility of the each cycle was well-defined. The charging voltage typically did not exceed 4.5 V and no corrosion of the stainless steel battery case was observed. One possible reason for the absence of corrosion is the formation of the passivation film on the stainless steel case by the decomposition of ether-based electrolyte at voltages higher than 4 V.

2.4. Characterizations. All batteries were tested on an Arbin BT-2000 battery tester. After a certain number of cycles, the batteries were stopped in both discharged and charged states, disassembled inside the Ar-filled glovebox, and the electrodes were collected for analyses. To measure the current yield of Li_2O_2 (i.e., the fraction of current that accomplishes the formation of desired Li_2O_2 in the discharged electrodes), iodometric titration was used.[32] This method was recently proposed by McCloskey et al.[20] as an accurate technique and the details can be found in their report. Titration of the discharged electrodes was conducted within 1−2 h after the discharge to avoid aging of the electrodes because Li_2O_2 may slowly react with the electrolyte.[16,20,33] Also, the electrodes were not washed with DME to avoid loss of Li_2O_2. The presence of electrolyte salt was shown to have no effect on the titration results.[20] For the microscopic study, the electrodes were gently washed with three portions of DME to remove the electrolyte. Scanning electron microscopy (SEM) and energy dispersive X-ray spectroscopy (EDS) measurements were conducted using FEI Quanta 3D FEG and JEOL 5900 instruments. Transmission electron microscopy (TEM) work was performed with an FEI Titan environmental transmission electron microscope (FEI, Hillsboro, OR, U.S.A.) operated at 300 kV and equipped with Cs-corrected field emission gun, which allows 0.1 nm resolution in high-resolution mode. Samples were loaded onto a normal TEM carbon grid.

Cyclic voltammetry (CV) was conducted with a CHI 604D potentiostat in a one-compartment cell (three-neck, pear-shaped flask) using a three-electrode configuration with Ag/Ag^+ as the reference electrode (0.40 V vs standard hydrogen electrode) and a Pt foil as the counter electrode. Special care was taken to avoid moisture by placing the cell in the N_2-filled glovebox, and ultrahigh purity O_2 was continuously bubbled during the CV scans. Polished and dried glassy carbon strips and Ru-coated glassy carbon strips were used as working electrodes. Thin Ru films (10 nm) were deposited by DC reactive magnetron sputtering using a Mighty Mak cathode (MEIVAC) as the sputtering source and 99.9% pure Ru disk as the target. Deposition was performed in 100% Ar at 0.47 nm s^{-1} rate.

Mass spectroscopy of the gases evolved during the battery charging was tested in situ using an SRS RGA 200 instrument with helium as the carrying gas. Calibration was performed using 10, 100, and 200 ppm gas standards. Details were reported in the earlier report.[7] X-ray photoelectron spectroscopy (XPS) spectra were recorded with a Physical Electronics Quantera scanning X-ray microprobe. Ru 3d peaks at 284.0 and 280.0 eV were used for referencing the spectra

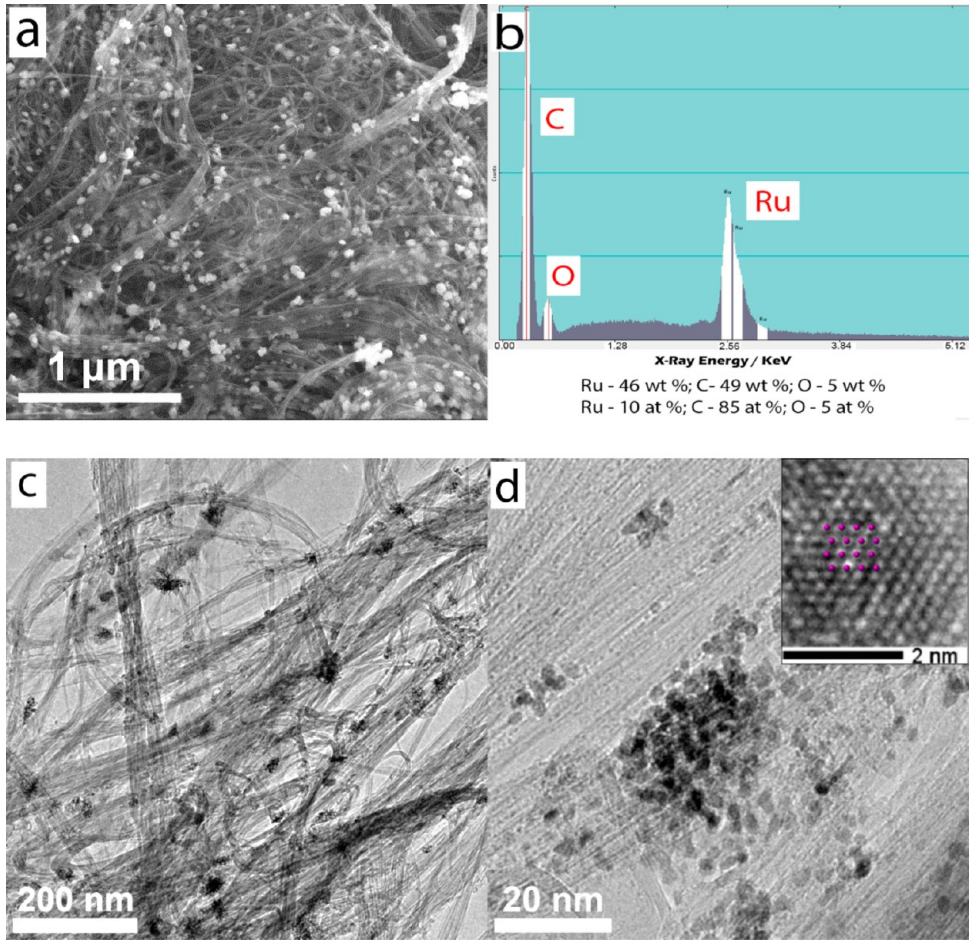

Figure 1. As prepared CNTs/Ru composite. (a) SEM image; (b) elemental composition by EDS; (c, d) TEM images at different magnifications; inset in d shows the high-resolution TEM image of a sinlge Ru nanoparticle.

together with F 1s peak of Lithion at 689.5 eV. The X-ray diffraction (XRD) pattern of the CNTs/Ru composite was recorded using a D8 Advance X-ray diffractometer (Bruker AXS, Inc.). Details for XPS and XRD measurements can be found in our previous report.[34]

3. RESULTS AND DISCUSSION

3.1. CNTs/Ru Composite. The selection of materials for fabricating the air electrode significantly impacts the cycling performance of Li−O_2 batteries. Carbon nanotubes (CNTs) are expected to be less reactive than high-surface-area mesoporous carbons (e.g., Ketjenblack) that have highly functionalized surfaces. Also, CNTs form an open network with a microporous structure, which simplifies morphological characterization. In a number of recent studies, ruthenium (Ru) and its oxygen-containing compounds were shown to be efficient catalysts for the oxygen evolution reaction (OER).[35−37] In the present study, CNTs decorated with Ru nanoparticles (i.e., CNTs/Ru nanocomposite) were mixed with lithiated Nafion (Lithion) to prepare air electrodes that then were used to examine the reversibility of Li_2O_2 formation/oxidation in a glyme-based electrolyte during the extended cycling of Li−O_2 batteries.

Morphology of the as prepared CNTs/Ru air electrode demonstrates uniform distribution of Ru nanoparticles in the CNTs network (Figure 1a). EDS analyses of wide areas reveals 46 wt % of Ru in the electrode (Figure 1b). Ru nanoparticles observed with SEM have an average diameter of ∼20 nm (Figure 1a). However, TEM indicates that these nanoparticles are actually aggregates of many smaller Ru nanoparticles with an average diameter of 2 nm (Figure 1c, d). High-resolution TEM of a single Ru nanoparticle in the inset of Figure 1d shows the [110] zone projection of the Ru crystal; the red dots in the inset show the atomic column positions in the model. The distance between the atomic columns in the horizontal direction is 2.36 Å. The presence of Ru in CNTs/Ru composite is also confirmed by the X-ray diffraction (XRD) pattern (see Figure S1 and corresponding text in Supporting Information).

3.2. Battery Performance. Voltage profiles of the Li−O_2 battery using the CNTs/Ru electrode and 1.0 M lithium trifluoromethanesulfonate in tetraethylene glycol dimethyl ether (LiTf-tetraglyme) as the electrolyte are shown in Figure 2a. The cycling protocol was designed to fully utilize the maximum discharge capacity of Li−O_2 batteries and achieve efficient oxidation of discharge products. Discharge was run until a voltage drop was observed with the cutoff at 2.0 V, while charging was continued until the capacity reached the value recorded during the exactly previous discharge step. The battery retained 64% of its initial capacity after 50 full cycles. It is also worth noting that, in the present work, running 50 cycles typically took a month. This is a reasonably long time when compared to measurement times reported by other groups, which typically are only a few days because of either intentional limitation on the capacity or the intrinsic limitation of the air electrode.[27,28] This is a remarkable result for a carbon-based

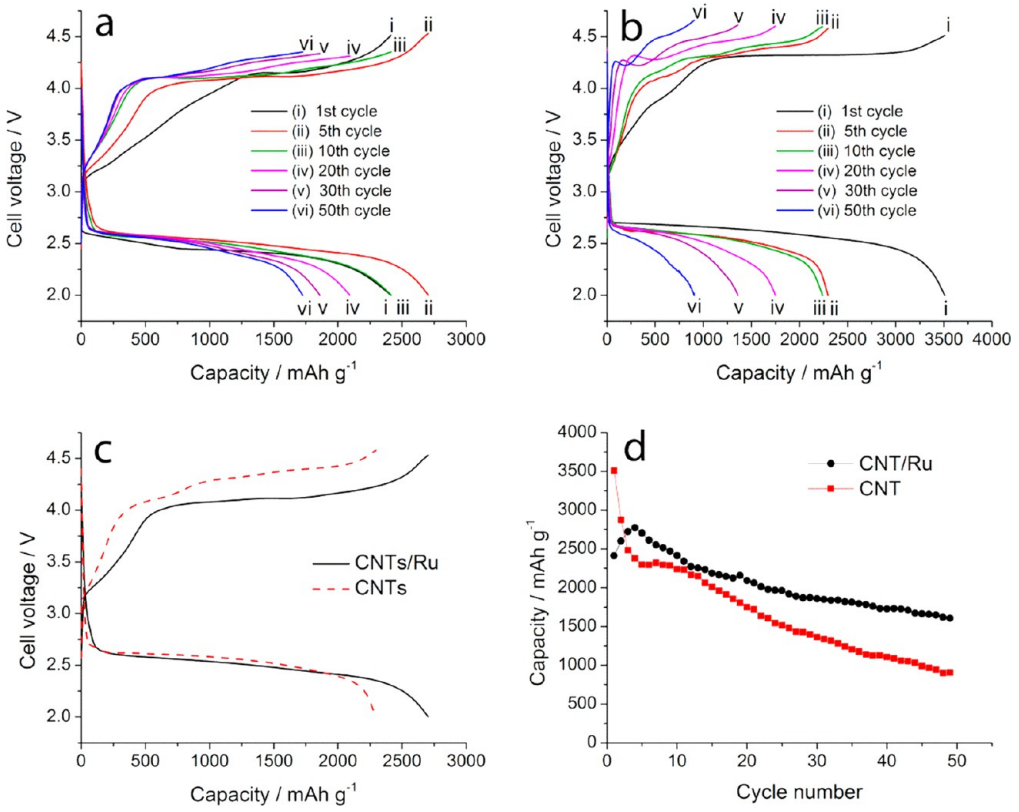

Figure 2. Voltage profiles of the cycled batteries with (a) CNTs/Ru electrodes and(b) CNTs electrodes. (c) Comparison of the 5th cycle voltage profiles recorded for the bateries with CNTs/Ru and CNTs electrodes. (d) Cycling performance of the batteries with CNTs/Ru electrodes and CNTs electrodes. The electrolyte is LiTf-tetraglyme. Capacity is calculated per total weight of CNTs and Ru for CNTs/Ru electrodes and per CNTs weight for CNTs electrodes.

electrode cycled under full discharge/charge conditions. However, the prolonged cycling shown in Figure 2a may not represent fully reversible Li−O_2 reactions. Instead, it could be the result of more efficient decomposition of both Li_2O_2 and the side products during the charging process. As can be seen from Figure 2a, the charging voltage plateau remains almost unchanged as cycling proceeds, and most of the charging happens within the range 4.1−4.3 V. Also, a steep increase of voltage is observed at the end of the charging process during the first five cycles. When a constant current was used during the charging process, anodic decomposition of electrolyte normally occurs at a constant voltage plateau.[38] Therefore, a steep increase in the charging voltage indicates the ending point of the decomposition of the discharge products. It should be noted that some of the discharge products, such as Li_2CO_3, are decomposed at a voltage higher than 4.3 V and CO_2 is released.[20] In addition to the CNTs/Ru electrodes, as a comparative study, we examined the performance of a Li−O_2 battery using a bare CNTs electrode without the Ru catalyst. Comparing parts a and b of Figure 2, it can be seen that the air electrode containing Ru nanoparticles exhibits a charging voltage 200−300 mV lower than that of the electrode without Ru nanoparticles (e.g., see Figure 2c for direct comparison of the voltage profiles recorded for the fifth cycle), indicating that Ru does promote the oxidation of discharge products. A slight increase in the discharge voltage for the electrode without Ru catalyst can be attributed to the higher CNTs loading (CNTs/Ru electrodes contained 46 wt % of Ru). Figure 2d indicates better capacity retention for the electrode with Ru nanoparticles because of the more efficient decomposition of the side products during the charging step.

3.3. Analysis of Discharge and Charge Products. Several studies have shown that Li_2O_2 forms toroidal or disk-shaped particles in discharged electrodes. This characteristic morphology is mostly related to the current density and seems to be irrelevant to electrolytes and carbon materials used for electrode fabrication.[39] With the help of TEM, the morphology of the discharge products formed during the first few shallow (i.e., capacity-limited) cycles also has been reported.[18] The main objective of the present study is to reveal the morphological evolution of discharge products formed during the extended cycling of the Li−O_2 battery with the LiTf-tetraglyme electrolyte. Figure 3 shows SEM images of the discharged CNTs/Ru electrodes at different cycle numbers. The pristine CNTs/Ru electrode has an abundance of Ru nanoparticles (Figure 3a). As shown in Figure 3b, toroidal particles with a more or less regular shape and an average diameter of 500 nm are observed after the first discharge. Careful analysis of the discharged electrode also reveals the presence of other minor nanostructures such as needle-like and plate-like crystallites (see Figure S2 and corresponding text in Supporting Information). There is a drastic change in the morphology of the discharge products from toroidal particles to a dense and smooth layer as soon as after the second discharge (Figure 3c−h). The layer is semitransparent to the electron beam as Ru nanoparticles and CNTs contours can be seen. The thickness of the layer varies from area to area, but it always forms a dense deposit without any distinct morphological features. It is important that, despite the obvious morphological

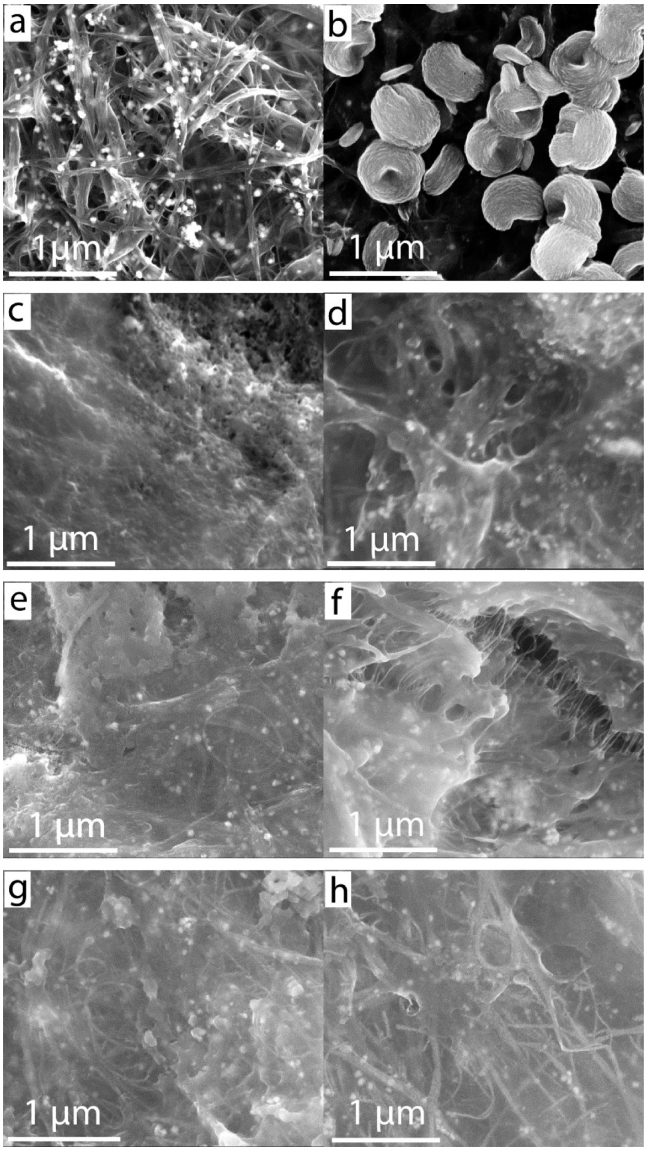

Figure 3. SEM images of (a) pristine electrode and discharged CNTs/Ru electrodes after (b) 1st, (c) 2nd, (d) 3rd, (e) 5th, (f) 10th, (g) 20th, and (h) 50th cycles in LiTf-tetraglyme electrolyte.

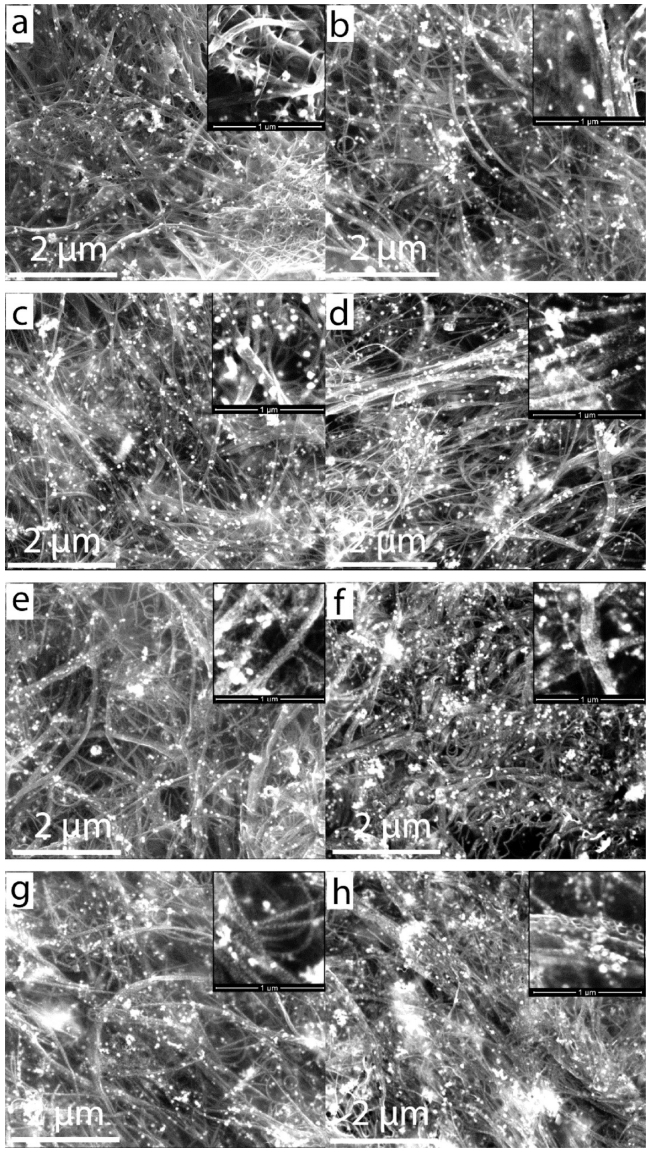

Figure 4. SEM images of (a) pristine CNTs/Ru electrode and charged CNTs/Ru electrodes after (b) 1st, (c) 2nd, (d) 3rd, (e) 5th, (f) 10th, (g) 20th, and (h) 50th cycles in LiTf-tetraglyme electrolyte.

changes in the very beginning, the character of the discharge products deposit does not change with further cycling.

After charging, almost all of the porosity of the electrodes is restored, and they are similar in appearance to the pristine electrode (Figure 4). This means that toroidal particles observed after the first discharge as well as the dense deposits of discharge products observed for subsequent cycle numbers are effectively decomposed, and thus, the discharge can be run for the next cycle. However, a closer look at the CNTs reveals changes on the surfaces even after the first charging (insets in Figure 4). The pristine CNTs have a smooth surface and bright spots corresponding to Ru nanoparticles (Figure 4a inset). The charged electrodes exhibit rough layers with grain-like morphologies as shown in the insets of Figure 4b–h. It has been reported that mesoporous carbons undergo severe decomposition during charging;[19,20] therefore, it is reasonable to assume that the observed layers could be a result of degradation of the CNTs as well as some deposits from electrolyte decomposition. High-resolution TEM imaging reveals a variety of crystalline particles of side products in networks of the CNTs and thin crystalline deposits on the surface of the CNTs in some areas (Supporting Information Figure S3).

We used X-ray photoelectron spectroscopy (XPS) to further analyze residues on the charged electrodes (Figure 5). The pristine electrode shows two Ru peaks at 284.0 (Ru $3d_{3/2}$) and 280.0 (Ru $3d_{5/2}$) eV[40] in addition to the C–F (C 1s) peak for Lithion at 292.9 eV[41] (Figure 5a). The former peak has a high energy shoulder due to the presence of CNTs. The latter peak is slightly shifted from the C–F peak for PTFE, which typically is observed at 292.5 eV[42] to 292.9 eV because of oxygen-containing groups present in the structure of Lithion.[43] In addition to these peaks, the C 1s spectra of charged electrodes demonstrate a series of peaks at 289.7, 287.5, and 285.5 eV (with slight shifts from sample to sample), which correspond to the observed layers on CNTs. The first group of peaks around 289.7 eV corresponds to C=O-containing species (i.e., carbonates,[44] lithium formate,[45] and lithium acetate[45]), the

dx.doi.org/10.1021/am503390q | ACS Appl. Mater. Interfaces 2014, 6, 14141–14151

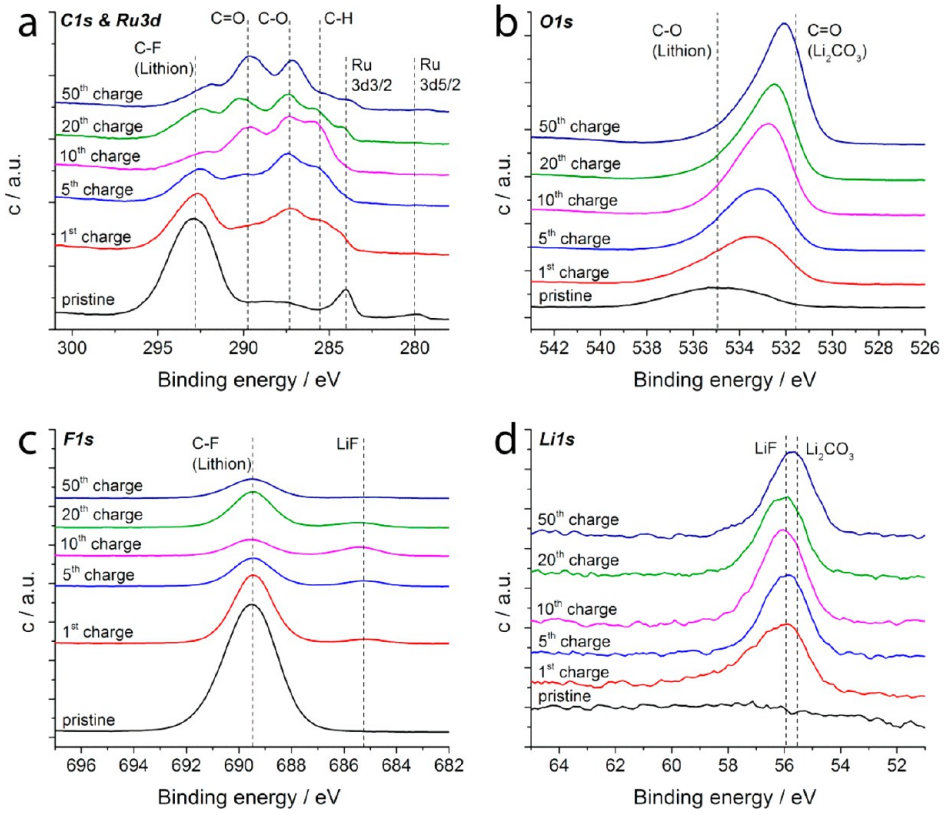

Figure 5. XPS results for the pristine and charged CNTs/Ru electrodes scanned in a) C 1s and Ru 3d, b) O 1s, and c) F 1s and d) Li 1s regions.

second group of peaks around 287.4 eV corresponds to C-O-containing species,[46−48] and the third group of peaks around 285.5 eV corresponds to C-H-containing species such as CH_3-group of lithium acetate.[45] Carbon electrodes decompose with the formation of carbonates[17−20] and cannot result in the second and third groups of peaks. Therefore, we believe that the layer on the CNTs mostly corresponds to the residue of the side products generated from decomposition of the electrolyte. However, we also observe that there is a consistent growth of the C═O (C 1s) peak with cycling and a consistent shift of the peak in the O 1s region from 535.0 eV (Lithion[41]) to lower binding energies (Figure 5b), both indicating the growing contribution from C═O-containing species as cycling proceeds. The F 1s spectra (Figure 5c) show a C-F peak for Lithion at 689.5 eV[43] and a LiF peak at 685.2 eV[49] from the decomposition of LiTf, which is the electrolyte salt.[14] The broad peak at ~55.7 eV in Li 1s spectra (Figure 5d) should be a result of superposition of lithium carbonates, lithium alkyl carbonates, lithium formate, lithium acetate, and LiF. It can be concluded from the XPS data that the observed deposits on the surface of CNTs after charging correspond to the residues of side products from the electrolyte decomposition with apparent contributions from the decomposition of CNTs.

Analysis of the thin layer remaining on the surface of CNTs after charging is of great importance because it switches the discharge from the predominant formation of Li_2O_2 to the predominant formation of side products as quantitatively shown below. The ratio of Li_2O_2 and the reaction side products reaches a stable value after the formation of this interfacial layer on the surface of CNTs. This clearly indicates the significance of interface in regards to the electrolyte stability. If this interfacial layer can promote decomposition of the electrolyte, one may expect that some other interfacial chemistry (e.g., noncarbon electrodes or modified carbon electrodes) may suppress it.

Although there are a variety of available spectroscopic methods to analyze discharge products in Li−O_2 batteries (XPS, FT-IR, XRD, etc.), they are not very quantitative. The aim of the present study is to quantify the contribution from desired reversible formation/oxidation of Li_2O_2 during the extended cycling. McCloskey et al. recently reported using iodometric titration of H_2O_2 to measure mg quantities of Li_2O_2.[20] This method was used in the present work and the results from control tests with commercial Li_2O_2 are provided in Supporting Information. Unfortunately, adding deionized water to the discharged CNTs/Ru electrodes caused disproportionation of peroxide with severe O_2 bubbling instead of the quantitative conversion of Li_2O_2 to H_2O_2 that is necessary for the titration. On the other hand, the discharged CNTs electrodes did not show disproportionation of peroxide, and the titration could be accomplished, indicating that Ru nanoparticles catalyze disproportionation of H_2O_2. The titration data for the discharged CNTs electrodes are summarized in Table 1. There is 70% current yield of Li_2O_2 (meaning that 70% of the charge passing through the cell was used to form Li_2O_2) after the first discharge but only 49 and 40% yields after the second and the third discharges, respectively. Interestingly, subsequent cycling up to the 50th cycle has little effect on the yield of Li_2O_2, which is consistent

Table 1. Current Yield of Li_2O_2 in the Discharged CNT Electrodes Collected after Various Cycles

cycle no.	1st	2nd	3rd	5th	10th	20th	50th
Li_2O_2 yield, %	70	49	40	33	33	42	40

dx.doi.org/10.1021/am503390q | ACS Appl. Mater. Interfaces 2014, 6, 14141−14151

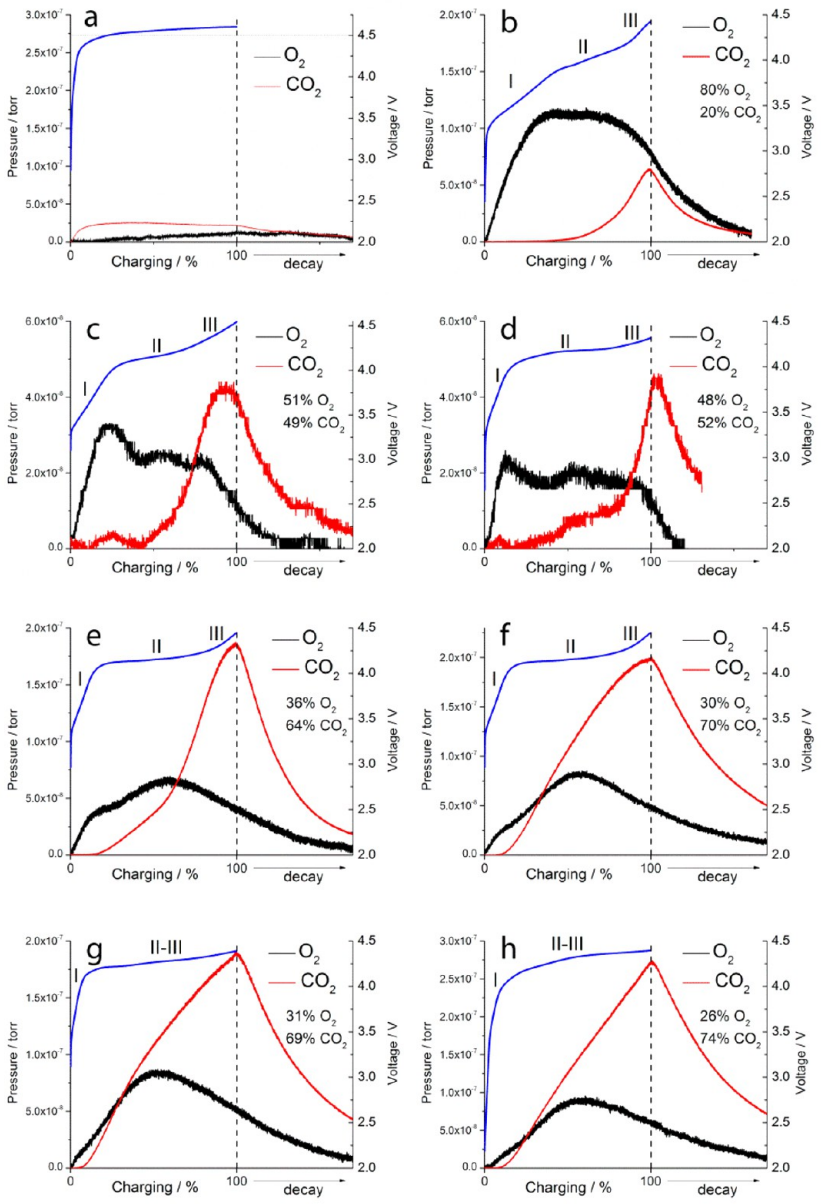

Figure 6. In situ mass spectroscopic analysis of O_2 and CO_2 evolved during (a) dummy charging of the battery with pristine undischarged CNTs/Ru electrode and charging of the batteries with CNTs/Ru electrodes for the (b) 1st, (c) 2nd, (d) 3rd, (e) 5th, (f) 10th, (g) 20th, and (h) 50th cycles. The electrolyte is LiTf-tetraglyme.

with the absence of any morphological changes as discussed earlier. This means that there is a drastic change in the discharge pathway only at the beginning of battery cycling, followed by the stabilization of the discharge pathway.

Mass spectroscopy was used for in situ analysis of the gases released during the charging process of the batteries, and the results are shown in Figure 6. As a control, the battery that was not discharged was subjected to dummy charging (Figure 6a). In this case, the charging voltage quickly exceeds 4.5 V and forms a plateau at about 4.55 V, corresponding to anodic decomposition of the electrolyte. This is accompanied by a release of only a small amount of CO_2. On the other hand, charging the actual cells at various cycle numbers results in a significant CO_2 release, while the voltage never exceeds 4.5 V (Figure 6b–h). However, this result does not exclude the indirect electrochemical decomposition of electrolyte and carbon through possible oxygen intermediates generated during Li_2O_2 oxidation.[19,20] The charging voltage profiles demonstrate three distinct regions for the first 10 cycles: region I is associated with release of O_2 only (oxidation of Li_2O_2), region II is associated with release of O_2/CO_2 (oxidation of Li_2O_2 and decomposition of side products), and region III is associated with a sharp increase in release of CO_2 (decomposition of side products). Regions II and III merge for the 20th and 50th cycles because of the higher polarization. Oxygen release significantly dominates over CO_2 release only during the first cycle charging and constitutes 80% of the total gas release (H_2 release from the Li anode was not counted). The O_2 contribution in the released gas drops to 51, 48, and 36% for the second, third, and fifth cycles, respectively. After the fifth cycle, only a slight decrease in O_2 release is observed (30, 31, and 26% O_2 contribution in the gases released during 10th, 20th, and 50th cycles, respectively). This once again confirms

dx.doi.org/10.1021/am503390q | ACS Appl. Mater. Interfaces 2014, 6, 14141−14151

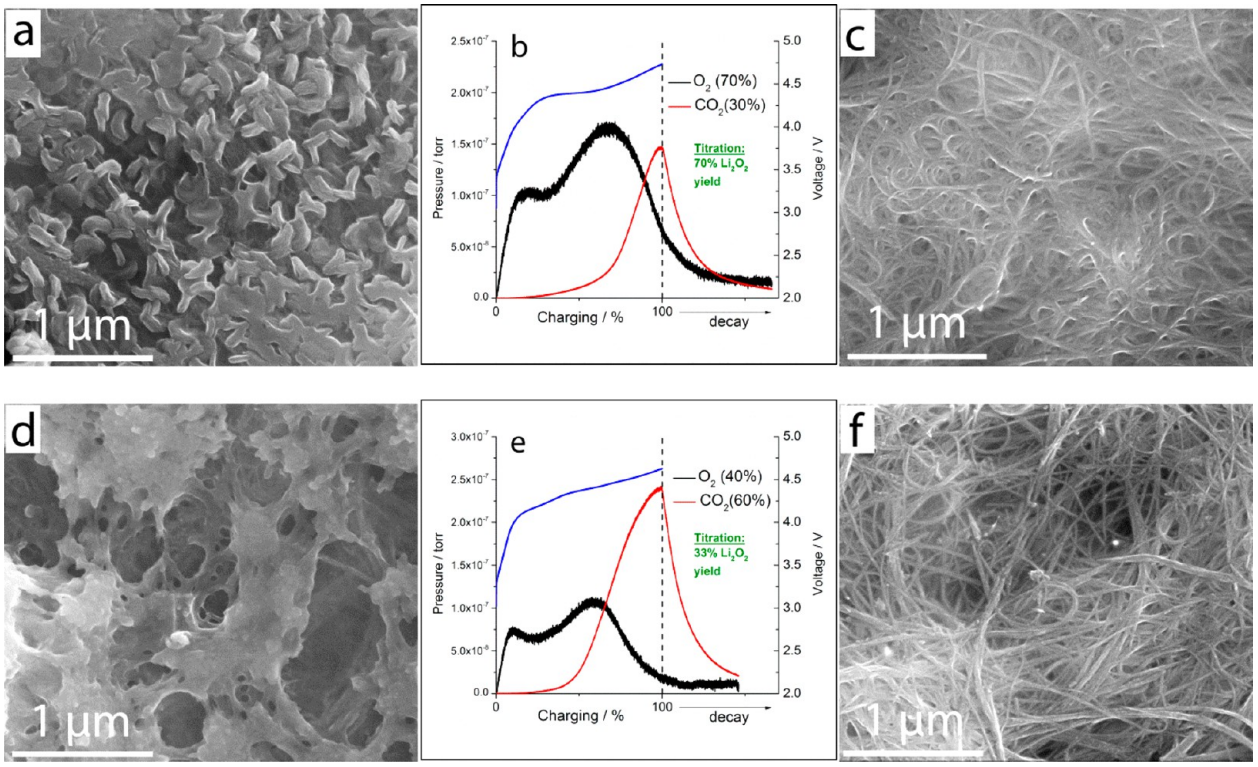

Figure 7. Results for the 1st (a, b, c) and 10th (d, e, f) cycles of the batteries with CNTs electrodes in LiTf-tetraglyme electrolyte. (a, d) SEM images of the discharged CNTs electrodes; (b, e) in situ mass spectroscopy analysis of O_2 and CO_2 evolved during charging; (c, f) SEM images of the charged CNTs electrodes.

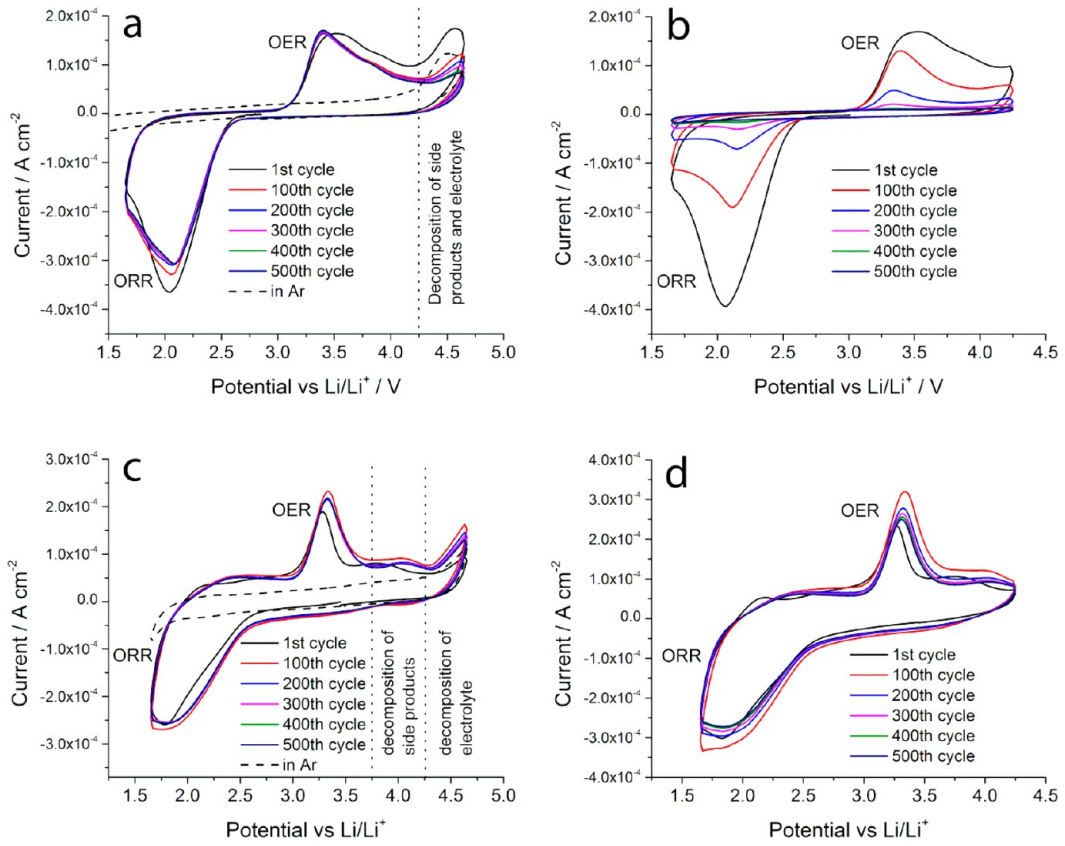

Figure 8. CV (100 mV s^{-1}) results for the flat (a, b) glassy carbon and (c, d) Ru electrodes recorded in LiTf-Tetraglyme electrolyte saturated with O_2.

the stabilization of electrochemical processes after the drastic change that occurs during the first few cycles of battery cycling.

We noticed that the observed phenomena are not specific to the CNTs/Ru electrodes. The same behavior is observed for CNTs electrodes without Ru although the cycling stability is not as good and the charging voltages are higher in this case (see Figure 2 for voltage profiles and cycling performance). After the first discharge, a layer of disk-shaped Li_2O_2 particles thoroughly coats the surface of CNTs electrodes (Figure 7a), and the titration gives 70% current yield of Li_2O_2 (see Table 1). The first-cycle charging results in 70% O_2 release (Figure 7b) and the porous structure of the CNTs electrode is restored as revealed by the SEM shown in Figure 7c. After the 10th discharge, a layer of deposit forms (Figure 7d) without any distinct nanostructures, and the titration reveals 33% current yield of Li_2O_2. The 10th cycle charging results in 40% O_2 release (Figure 7e), and again, the porous structure of CNTs electrode is restored (Figure 7f). Although a small portion of the CO_2 may be generated from the side reactions of CNTs and electrolyte during charging,[19,20] most of CO_2 is released from the side products generated during discharge.

Careful analysis on the mass spectroscopy data (Figure 7b, e) indicates that, although only O_2 release is observed in the beginning of charging, its amount is less than that observed in the middle of charging when CO_2 also is released. This important result is in agreement with the delithiation mechanism, which was hypothesized by Lu et al.[50] and recently supported with theoretical calculations by Kang et al.[51]

Prolonged battery cycling could not be achieved with mesoporous carbons such as Ketjenblack.[14] The use of CNTs is beneficial because of the increased porosity of the carbon network, which prevents clogging in the electrode by side products. Another explanation can be attributed to the better stability of CNTs compared to the highly functionalized reactive surfaces of carbons such as Ketjenblack.

3.4. Cyclic Voltammetry (CV) Study on the Origin of the Extended Cycling. In general, the long cycle life of the Li−O_2 battery tested in this study is the result of the appropriate material selection and the efficient charging process. It is important to efficiently decompose most of the discharge products (Li_2O_2 and side products) during the charging step in order to restore the porosity and the surface of the electrode for the next discharge cycle. The situation may also be complicated by side products generated from the decomposition of the electrolyte and degradation of CNTs during the charging process.[19,20] However, the contribution from the decomposition of the side products generated during discharge dominates the charge process. To efficiently decompose the side products, the charging voltage of the batteries in this study was not limited, and charging was continued until capacity reached the same value observed for the previous discharge step.

To further support the results described above, cyclic voltammetry testing on glassy carbon and Ru-coated glassy carbon electrodes was performed over different ranges as shown in Figure 8. The cathodic peaks are attributed to the oxygen reduction reaction (ORR) and formation of a continuous solid layer of Li_2O_2 and side products (see also Figure S4 and corresponding text in Supporting Information). The corresponding anodic peaks are attributed to the oxygen evolution reaction (OER), that is, the oxidation of Li_2O_2 and decomposition of side products at higher potentials.

The area above 4.25 V is of particular importance. Although the scan to 4.75 V in Figure 8a involves the anodic decomposition of the electrolyte, it also results in an efficient decomposition of side products erasing the electrode surface. Such regime allows unrestricted cycling and represents idealization of the battery operation. One should keep in mind, however, that this cycling is not truly reversible because it involves continuous decomposition of the electrolyte and thus is limited by its amount. On the other hand, setting the anodic limit to 4.25 V results in continuous accumulation of side products on the electrode surface and thus limits the cycle life (Figure 8b).

CV on Ru coated glassy carbon electrode in Figure 8c, d also results in ORR and OER peaks similarly to the cycling on glassy carbon but with certain changes due to the catalytic activity of Ru (see Supporting Information Figure S5 and corresponding discussion). Anodic current in the range 3.75−4.25 V can be attributed to the decomposition of side products while the anodic current above 4.25 V corresponds to the electrolyte decomposition (Figure 8c). Decomposition of side products is shifted to a lower potential on Ru surface compared to glassy carbon and is separated from the electrolyte decomposition. Therefore, setting the voltage limit to 4.25 V for cycling on Ru is sufficient for the complete decomposition of Li_2O_2 and the side products leading to the stable CV curves (Figure 8d).

Another feature of the cycling on glassy carbon and on Ru electrodes is a relatively low ratio of OER/ORR peak areas. In other words, the charge passed through the cell during ORR step is higher than that during the following OER step. In the case of glassy carbon electrode, the OER peak area is about 60% of the ORR peak (from Figure 8a) while in the case of Ru electrode it is only about 30% (from Figure 8c). Such a low ratio is explained by the flat geometry of the electrodes and excess of the electrolyte. Only a portion of the discharge products forms a solid layer on the flat electrode surface while other portion migrates to the electrolyte and therefore is not oxidized during the following charging step. In the case of Ru, most of the discharge products migrate to the electrolyte apparently due to the poor adherence to Ru surface (see Figure S6 and corresponding text in Supporting Information).

4. CONCLUSIONS

The extended cycling behavior of Li−O_2 batteries based on CNTs was investigated by various approaches. Important conditions that lead to long cyclability are appropriate material selection and an efficient charging protocol to achieve efficient decomposition of discharge products including Li_2O_2 and side products. When used in Li−O_2 batteries, CNTs/Ru electrodes can maintain more than 50 full discharge−charge cycles without a sharp decrease in capacity. Analysis of the discharge/charge products during the cycling process reveals predominant formation of the desired Li_2O_2 for only the first cycle. After a few cycles, a stable interfacial layer forms on the surfaces of the CNTs (mainly from decomposition of the LiTf-tetraglyme electrolyte and partially from the side reaction of CNTs). This interfacial layer cannot be decomposed during subsequent charging process and it switches reactions occurring during discharging from the predominant formation of Li_2O_2 to the predominant formation of side products. Interestingly, after this drastic change in the first few cycles of battery cycling, the yield of Li_2O_2 in the reaction products stabilizes at about 33−40% for the subsequent cycles. The reported observations are, in general, not limited to the presence of Ru, and the same

transformations in discharge/charge products are also observed on bare CNT electrodes. Further investigation on the interfacial layer which in situ forms on air electrode may increase the long-term yield of Li_2O_2 during the cycling and enable highly reversible Li−O_2 batteries required for practical applications.

■ ASSOCIATED CONTENT

Supporting Information

Additional data (figures and discussion). This material is available free of charge via the Internet at http://pubs.acs.org.

■ AUTHOR INFORMATION

Corresponding Authors

*Email: wu.xu@pnnl.gov.
*Email: jiguang.zhang@pnnl.gov.

Notes

The authors declare no competing financial interest.

■ ACKNOWLEDGMENTS

This work was supported by the Assistant Secretary for Energy Efficiency and Renewable Energy, Office of Vehicle Technologies, of the U.S. Department of Energy (DOE). The microscopic analysis in this work was supported by the Joint Center for Energy Storage Research, an Energy Innovation Hub funded by DOE's Office of Science, Basic Energy Sciences, and was performed in the William R. Wiley Environmental Molecular Sciences Laboratory, a national scientific user facility sponsored by the DOE's Office of Biological and Environmental Research and located at Pacific Northwest National Laboratory.

■ REFERENCES

(1) Park, M.; Sun, H.; Lee, H.; Lee, J.; Cho, J. Lithium−Air Batteries: Survey on the Current Status and Perspectives Towards Automotive Applications from a Battery Industry Standpoint. *Adv. Energy Mater.* **2012**, *2*, 780−800.

(2) Girishkumar, G.; McCloskey, B.; Luntz, A. C.; Swanson, S.; Wilcke, W. Lithium−Air Battery: Promise and Challenges. *J. Phys. Chem. Lett.* **2010**, *1*, 2193−2203.

(3) Abraham, K. M.; Jiang, Z. A Polymer Electrolyte - Based Rechargeable Lithium/Oxygen Battery. *J. Electrochem. Soc.* **1996**, *143*, 1−5.

(4) Laoire, C. O.; Mukerjee, S.; Abraham, K. M.; Plichta, E. J.; Hendrickson, M. A. Elucidating the Mechanism of Oxygen Reduction for Lithium−Air Battery Applications. *J. Phys. Chem. C* **2009**, *113*, 20127−20134.

(5) Mizuno, F.; Nakanishi, S.; Kotani, Y.; Yokoishi, S.; Iba, H. Rechargeable Li−Air Batteries with Carbonate-Based Liquid Electrolytes. *Electrochemistry* **2010**, *78*, 403−405.

(6) Freunberger, S. A.; Chen, Y.; Peng, Z.; Griffin, J. M.; Hardwick, L. J.; Barde, F.; Novak, P.; Bruce, P. G. Reactions in the Rechargeable Li−O_2 Battery with Alkyl Carbonate Eelectrolytes. *J. Am. Chem. Soc.* **2011**, *133*, 8040−8047.

(7) Xu, W.; Viswanathan, V. V.; Wang, D.; Towne, S. A.; Xiao, J.; Nie, Z.; Hu, D.; Zhang, J.-G. Investigation on the Charging Process of Li_2O_2-Based Air Electrodes in Li−O_2 Batteries with Organic Carbonate Electrolytes. *J. Power Sources* **2011**, *196*, 3894−3899.

(8) Laoire, C. O.; Mukerjee, S.; Abraham, K. M.; Plichta, E. J.; Hendrickson, M. A. Influence of Nonaqueous Solvents on the Electrochemistry of Oxygen in the Rechargeable Lithium−Air Battery. *J. Phys. Chem. C* **2010**, *114*, 9178−9186.

(9) Freunberger, S. A.; Chen, Y.; Drewett, N. E.; Hardwick, L. J.; Barde, F.; Bruce, P. G. The Lithium−Oxygen Battery with Ether-Based Eelectrolytes. *Angew. Chem., Int. Ed. Engl.* **2011**, *50*, 8609−8613.

(10) McCloskey, B. D.; Bethune, D. S.; Shelby, R. M.; Girishkumar, G.; Luntz, A. C. Solvents' Critical Role in Nonaqueous Lithium−Oxygen Battery Electrochemistry. *J. Phys. Chem. Lett.* **2011**, *2*, 1161−1166.

(11) McCloskey, B. D.; Bethune, D. S.; Shelby, R. M.; Mori, T.; Scheffler, R.; Speidel, A.; Sherwood, M.; Luntz, A. C. Limitations in Rechargeability of Li-O_2 Batteries and Possible Origins. *J. Phys. Chem. Lett.* **2012**, *3*, 3043−3047.

(12) Bryantsev, V. S.; Uddin, J.; Giordani, V.; Walker, W.; Addison, D.; Chase, G. V. The Identification of Stable Solvents for Nonaqueous Rechargeable Li-Air Batteries. *J. Electrochem. Soc.* **2013**, *160*, A160−A171.

(13) Bryantsev, V. S.; Giordani, V.; Walker, W.; Blanco, M.; Zecevic, S.; Sasaki, K.; Uddin, J.; Addison, D.; Chase, G. V. Predicting Solvent Stability in Aprotic Electrolyte Li−Air Batteries: Nucleophilic Substitution by the Superoxide Anion Radical ($O_2^{\bullet-}$). *J. Phys. Chem. A* **2011**, *115*, 12399−12409.

(14) Nasybulin, E.; Xu, W.; Engelhard, M. H.; Nie, Z.; Burton, S. D.; Cosimbescu, L.; Gross, M. E.; Zhang, J.-G. Effects of Electrolyte Salts on the Performance of Li−O_2 Batteries. *J. Phys. Chem. C* **2013**, *117*, 2635−2645.

(15) Veith, G. M.; Nanda, J.; Delmau, L. H.; Dudney, N. J. Influence of Lithium Salts on the Discharge Chemistry of Li−Air Cells. *J. Phys. Chem. Lett.* **2012**, *3*, 1242−1247.

(16) Younesi, R.; Hahlin, M.; Björefors, F.; Johansson, P.; Edström, K. Li−O_2 Battery Degradation by Lithium Peroxide (Li_2O_2): A Model Study. *Chem. Mater.* **2012**, *25*, 77−84.

(17) McCloskey, B. D.; Speidel, A.; Scheffler, R.; Miller, D. C.; Viswanathan, V.; Hummelshøj, J. S.; Nørskov, J. K.; Luntz, A. C. Twin Problems of Interfacial Carbonate Formation in Nonaqueous Li−O_2 Batteries. *J. Phys. Chem. Lett.* **2012**, *3*, 997−1001.

(18) Gallant, B. M.; Mitchell, R. R.; Kwabi, D. G.; Zhou, J.; Zuin, L.; Thompson, C. V.; Shao-Horn, Y. Chemical and Morphological Changes of Li−O_2 Battery Electrodes upon Cycling. *J. Phys. Chem. C* **2012**, *116*, 20800−20805.

(19) Ottakam Thotiyl, M. M.; Freunberger, S. A.; Peng, Z.; Bruce, P. G. The Carbon Electrode in Nonaqueous Li-O_2 Cells. *J. Am. Chem. Soc.* **2013**, *135*, 494−500.

(20) McCloskey, B. D.; Valery, A.; Luntz, A. C.; Gowda, S. R.; Wallraff, G. M.; Garcia, J. M.; Mori, T.; Krupp, L. E. Combining Accurate O_2 and Li_2O_2 Assays to Separate Discharge and Charge Stability Limitations in Nonaqueous Li−O_2 Batteries. *J. Phys. Chem. Lett.* **2013**, *4*, 2989−2993.

(21) Nasybulin, E.; Xu, W.; Engelhard, M. H.; Nie, Z.; Li, X. S.; Zhang, J.-G. Stability of Polymer Binders in Li−O_2 Batteries. *J. Power Sources* **2013**, *243*, 899−907.

(22) Black, R.; Oh, S. H.; Lee, J. H.; Yim, T.; Adams, B.; Nazar, L. F. Screening for Superoxide Reactivity in Li-O_2 Batteries: Effect on Li_2O_2/LiOH Crystallization. *J. Am. Chem. Soc.* **2012**, *134*, 2902−2905.

(23) Younesi, R.; Hahlin, M.; Treskow, M.; Scheers, J.; Johansson, P.; Edström, K. Ether Based Electrolyte, $LiB(CN)_4$ Salt and Binder Degradation in the Li−O_2 Battery Studied by Hard X-ray Photoelectron Spectroscopy (HAXPES). *J. Phys. Chem. C* **2012**, *116*, 18597−18604.

(24) Jung, H.-G.; Hassoun, J.; Park, J.-B.; Sun, Y.-K.; Scrosati, B. An Improved High-Performance Lithium−Air Battery. *Nat. Chem.* **2012**, *4*, 579−585.

(25) Xu, J.-J.; Xu, D.; Wang, Z.-L.; Wang, H.-G.; Zhang, L.-L.; Zhang, X.-B. Synthesis of Perovskite-Based Porous $La_{0.75}Sr_{0.25}MnO_3$ Nanotubes as a Highly Efficient Electrocatalyst for Rechargeable Lithium−Oxygen Batteries. *Angew. Chem., Int. Ed. Engl.* **2013**, *52*, 3887−3890.

(26) Ryu, W.-H.; Yoon, T.-H.; Song, S. H.; Jeon, S.; Park, Y.-J.; Kim, I.-D. Bifunctional Composite Catalysts Using Co_3O_4 Nanofibers Immobilized on Nonoxidized Graphene Nanoflakes for High-Capacity and Long-Cycle Li−O_2 Batteries. *Nano Lett.* **2013**, *13*, 4190−4197.

(27) Ottakam Thotiyl, M. M.; Freunberger, S. A.; Peng, Z.; Chen, Y.; Liu, Z.; Bruce, P. G. A Stable Cathode for the Aprotic Li−O_2 Battery. *Nat. Mater.* **2013**, *12*, 1050−1056.

(28) Peng, Z.; Freunberger, S. A.; Chen, Y.; Bruce, P. G. A Reversible and Higher-Rate Li-O_2 Battery. *Science* **2012**, *337*, 563−566.
(29) Hirsch, A.; Vostrowsky, O. In *Functional Molecular Nanostructures*; Schlüter, A. D., Ed.; Springer: Berlin Heidelberg, 2005; Vol. *245*, pp 193−237.
(30) Lu, J. Effect of Surface Modifications on the Decoration of Multiwalled Carbon Nanotubes with Ruthenium Nanoparticles. *Carbon* **2007**, *45*, 1599−1605.
(31) Selvaraj, V.; Vinoba, M.; Alagar, M. Electrocatalytic Oxidation of Ethylene Glycol on Pt and Pt−Ru Nanoparticles Modified Multiwalled Carbon Nanotubes. *J. Colloid Interface Sci.* **2008**, *322*, 537−544.
(32) http://www.h2o2.com/technical-library/analytical-methods/default.aspx?pid=70&name=Iodometric-Titration (accessed Aug. 1, 2014).
(33) Assary, R. S.; Lau, K. C.; Amine, K.; Sun, Y.-K.; Curtiss, L. A. Interactions of Dimethoxy Ethane with Li2O2 Clusters and Likely Decomposition Mechanisms for Li−O_2 Batteries. *J. Phys. Chem. C* **2013**, *117*, 8041−8049.
(34) Xu, W.; Hu, J.; Engelhard, M. H.; Towne, S. A.; Hardy, J. S.; Xiao, J.; Feng, J.; Hu, M. Y.; Zhang, J.; Ding, F.; et al. The Stability of Organic Solvents and Carbon Electrode in Nonaqueous Li-O_2 Batteries. *J. Power Sources* **2012**, *215*, 240−247.
(35) Harding, J. R.; Lu, Y.-C.; Tsukada, Y.; Shao-Horn, Y. Evidence of Catalyzed Oxidation of Li2O2 for Rechargeable Li-Air battery Applications. *Phys. Chem. Chem. Phys.* **2012**, *14*, 10540−10546.
(36) Li, F.; Tang, D.-M.; Chen, Y.; Golberg, D.; Kitaura, H.; Zhang, T.; Yamada, A.; Zhou, H. Ru/ITO: A Carbon-Free Cathode for Nonaqueous Li−O_2 Battery. *Nano Lett.* **2013**, *13*, 4702−4707.
(37) Yilmaz, E.; Yogi, C.; Yamanaka, K.; Ohta, T.; Byon, H. R. Promoting Formation of Noncrystalline Li_2O_2 in the Li−O_2 Battery with RuO_2 Nanoparticles. *Nano Lett.* **2013**, *13*, 4679−4684.
(38) Nasybulin, E.; Xu, W.; Engelhard, M. H.; Li, X. S.; Gu, M.; Hu, D.; Zhang, J.-G. Electrocatalytic Properties of Poly(3,4-ethylenedioxythiophene) (PEDOT) in Li-O_2 Battery. *Electrochem. Commun.* **2013**, *29*, 63−66.
(39) Lu, Y.-C.; Gallant, B. M.; Kwabi, D. G.; Harding, J. R.; Mitchell, R. R.; Whittingham, M. S.; Shao-Horn, Y. Lithium-Oxygen Batteries: Bridging Mechanistic Understanding and Battery Performance. *Energy Environ. Sci.* **2013**, *6*, 750−768.
(40) Hrbek, J. Carbonaceous Overlayers on Ru (001). *J. Vac. Sci. Technol., A* **1986**, *4*, 86−89.
(41) Schulze, M.; Lorenz, M.; Wagner, N.; Gülzow, E. XPS Analysis of the Degradation of Nafion. *Fresenius' J. Anal. Chem.* **1999**, *365*, 106−113.
(42) Taylor, J. A.; Lancaster, G. M.; Rabalais, J. W. Surface Alteration of Graphite, Graphite Monofluoride, and Teflon by Interaction with Ar^+ and Xe^+ Beams. *Appl. Surf. Sci.* **1978**, *1*, 503−514.
(43) Hoffmann, E. A.; Fekete, Z. A.; Korugic-Karasz, L. S.; Karasz, F. E.; Wilusz, E. Theoretical and Experimental X-ray Photoelectron Spectroscopy Investigation of Ion-Implanted Nafion. *J. Polym. Sci., Part A: Polym. Chem.* **2004**, *42*, 551−556.
(44) Contarini, S.; Rabalais, J. W. Ion Bombardment-Induced Decomposition of Li and Ba Sulfates and Carbonates Studied by X-ray Photoelectron Spectroscopy. *J. Electron Spectrosc. Relat. Phenom.* **1985**, *35*, 191−201.
(45) Wulser, K. W.; Langell, M. A. Carboxylic Acid Adsorption on NiO(100) Characterized by X-ray Photoelectron and High Resolution Electron Energy Loss Spectroscopies. *Catal. Lett.* **1992**, *15*, 39−50.
(46) Briggs, D.; Beamson, G. Primary and Secondary Oxygen-Induced C1s Binding Energy Shifts in X-ray Photoelectron Spectroscopy of Polymers. *Anal. Chem.* **1992**, *64*, 1729−1736.
(47) Boulanger, P.; Riga, J.; Delhalle, J.; Verbist, J. J. An XPS Study of Hexagonal Polyoxymethylene with Various Bulk Morphologies: Surface Modification Under X-ray Exposure. *Polymer* **1988**, *29*, 797−801.
(48) Itkis, D. M.; Semenenko, D. A.; Kataev, E. Y.; Belova, A. I.; Neudachina, V. S.; Sirotina, A. P.; Hävecker, M.; Teschner, D.; Knop-Gericke, A.; Dudin, P.; et al. Reactivity of Carbon in Lithium−Oxygen Battery Positive Electrodes. *Nano Lett.* **2013**, *13*, 4697−4701.
(49) Morgan, W. E.; Van Wazer, J. R.; Stec, W. J. Inner-Orbital Photoelectron Spectroscopy of the Alkali Metal Halides, Perchlorates, Phosphates, and Pyrophosphates. *J. Am. Chem. Soc.* **1973**, *95*, 751−755.
(50) Lu, Y.-C.; Shao-Horn, Y. Probing the Reaction Kinetics of the Charge Reactions of Nonaqueous Li−O_2 Batteries. *J. Phys. Chem. Lett.* **2012**, *4*, 93−99.
(51) Kang, S.; Mo, Y.; Ong, S. P.; Ceder, G. A Facile Mechanism for Recharging Li_2O_2 in Li−O_2 Batteries. *Chem. Mater.* **2013**, *25*, 3328−3336.